# Fluorescence component in the reflectance spectra from coastal waters. Dependence on water composition

**A. Gilerson[1], J. Zhou[1], S. Hlaing[1], I. Ioannou[1], J. Schalles[2], B. Gross[1], F. Moshary[1], and S. Ahmed[1*]**

[1]*Optical Remote Sensing Laboratory, Department of Electrical Engineering, The City College of the City University of New York, 140 St & Convent Ave, New York, NY, 1003 USA*
[2]*Biology Department, Creighton University, 2500 California Plaza, Omaha, NE 68178 USA*
**Corresponding author: ahmed@ccny.cuny.edu*

**Abstract:** Based on HYDROLIGHT simulations of more than 2000 reflectance spectra from datasets typical of coastal waters with highly variable optically active constituents as well as on intercomparisons with field measurements, the magnitude of chlorophyll fluorescence was analyzed and parameterized as a function of phytoplankton, CDOM, and suspended inorganic matter concentrations. Using the parameterizations developed, we show that variations in the fluorescence component of water leaving radiance in coastal waters are due more to the variability of attenuation in the water than to the variability of the fluorescence quantum yield, which we estimate to be relatively stable at around 1%. Finally, the ranges of water conditions where fluorescence plays a significant role in the reflectance NIR peak and where it is effectively undetectable are also determined.



**OCIS codes:** (010.4450) Ocean Optics; (280.0280) Remote sensing

## References and links

1. R. M. Letelier and M. R. Abbott, "An analysis of Chlorophyll Fluorescence Algorithms for the Moderate Resolution Imaging Spectrometer (MODIS)," Remote Sens. Environ. **58**, 215-223 (1996).
2. Y. Huot, C. A. Brown, and J. J. Cullen, "New algorithms for MODIS sun-induced chlorophyll fluorescence and a comparison with present data products," Limnol. Oceanogr. Methods **3**, 108 – 130 (2005).
3. C. Hu, F. E. Muller-Karger, C. J. Taylor, K. L. Carder, C. Kelble, E. Johns, and C. A. Heil, "Red tide detection and tracing using MODIS fluorescence data: A regional example in SW Florida coastal waters," Remote Sens. Environ. **97**, 311-321 (2005).
4. J. F. R. Gower, R. Doerffer, and G. A. Borstad, "Interpretation of the 685 nm peak in water-leaving radiance spectra in terms of fluorescence, absorption and scattering, and its observation by MERIS," Int. J. Remote Sens. **20**, 1771-1786 (1999).
5. G. Dall'Olmo, A. A. Gitelson, D. C. Rundquist, B. Leavitt, T. Barrow and J. C. Holz, "Assessing the potential of SeaWiFS and MODIS for estimating chlorophyll concentration in turbid productive waters using red and near-infrared bands," Remote Sens. Environ. **96**, 176-187 (2005).
6. S. Ahmed, A. Gilerson, J. Zhou, J. Chowdhary, I. Ioannou, R. Amin, B. Gross, and F. Moshary, "Evaluation of the impact of backscatter spectral characteristics on Chl retrievals in coastal waters," Proc. SPIE **6406** (2006).
7. A. A. Gitelson, J. F. Schalles, and C. M. Hladik, "Remote chlorophyll-a retrieval in turbid, productive estuaries: Chesapeake Bay case study," Remote Sens. Environ. **109**, 464-472 2007.
8. S. R. Laney, R. M. Letelier, and M. R. Abbott, "Parameterizing the natural fluorescence kinetics of Thalassiosira weissflogii," Limnol. Oceanogr. **50**, 1499-1510 (2005).
9. J. F. Schalles, "Optical Remote Sensing techniques to estimate Phytoplankton Chlorophyll a concentrations in coastal waters with varying suspended matter and CDOM concentrations," in *Remote Sensing of Aquatic Coastal Ecosystem Processes: Science and Management Applications*, L. L. Richardson and E. F. LeDrew, eds. (Springer, 2006), Chap. 3.
10. S. Ahmed, A. Gilerson, A. Gill, B. M. Gross, F. Moshary, J. Zhou, "Separation of fluorescence and elastic scattering from algae in seawater using polarization discrimination," Opt. Commun. **235**, 23-30 (2004).

#87554 - $15.00 USD Received 14 Sep 2007; revised 6 Nov 2007; accepted 6 Nov 2007; published 12 Nov 2007

11. A. Gilerson, J. Zhou, M. Oo, J. Chowdhary, B. Gross, F. Moshary, and S. Ahmed, "Retrieval of fluorescence from reflectance spectra of algae in sea water through polarization discrimination: modeling and experiments," Appl. Opt. **45**, 5568-5581 (2006).
12. R. A. Arnone, Z. P. Lee, P. Martinolich, B. Casey, and S. D. Ladner, "Characterizing the optical properties of coastal waters by coupling 1 km and 250 m channels on MODIS – Terra," in Proc. Ocean Optics XVI, Santa Fe, New Mexico (2002).
13. M. Wang and W. Shi, "Estimation of ocean contribution at the MODIS near-infrared wavelengths along the east coast of the U.S.: Two case studies," Geophys. Res. Lett. **32**, L13606 (2005).
14. B. Franz, "MODIS Land Bands for Ocean Remote Sensing: Application to Chesapeake Bay," presented at the MODIS Science Team Meeting, College Park, MD, Oct., 2006.
15. M. Babin, A. Morel and B. Gentili, "Remote sensing of sea surface Sun-induced chlorophyll fluorescence: consequences of natural variations in the optical characteristics of phytoplankton and the quantum yield of chlorophyll a fluorescence," Int. J. Remote Sens. **17**, 2417-2448 (1996).
16. Z. Lee, K. L. Carder, R. Arnone, "Deriving inherent optical properties from water color: a multiband quasi-analytical algorithm for optically deep water," Appl. Opt. **41**, 5755-5772 (2002).
17. J. Fischer and U. Kronfeld, "Sun-stimulated chlorophyll fluorescence. 1. Influence of oceanic properties," Int. J. Remote Sens. **11**, 2125-2147 (1990).
18. J. F. R. Gower, L. Brown, and G. A. Borstad, "Observation of chlorophyll fluorescence in west coast waters of Canada using the MODIS satellite sensor, "Can. J. Remote Sens. **30**, 17-25 (2004).
19. C. S. Roesler and M. J. Perry, "In situ phytoplankton absorption, fluorescence emission, and particulate backscattering spectra determined from reflectance," J. Geophys. Res. **100**, C7, 13279-13294 (1995).
20. C. D. Mobley, *Light and Water. Radiative Transfer in Natural Waters* (Academic Press, New York, 1994).
21. C. D. Mobley and L. K. Sundman, HYDROLIGHT 4.2, Sequoia Scientific, Inc. (2001).
22. R. R. Bidigare, M. E. Ondrusek, J. H. Morrow, and D. A. Kiefer, "In vivo absorption properties of algal pigments," Proc. SPIE Ocean Optics X **1302**, 290-302 (1990).
23. S. Ahmed, A. Gilerson, J. Zhou, I. Ioannou, B. Gross, and F. Moshary, "Impact of apparent fluorescence shift on retrieval Algorithms for coastal waters," in Proc. Ocean Optics XVIII, Montreal, Canada (2006).
24. Standard methods for the examination of water and wastewater (20th edition). Section 1200 – Chlorophyll. American Public Health Association, Washington, D.C. (1998).
25. M. Babin, D. Stramski, G. M. Ferrari, H. Claustre, A. Bricaud, G. Obolensky, and N. Hoepffner, "Variations in the light absorption coefficients of phytoplankton, non-algal particles, and dissolved organic matter in coastal waters around Europe," J. Geophys. Res. **108**, C7, 3211 10.1029/2001JC000882 (2003).
26. R. P. Bukata, J. H. Jerome, K. Y. Kondratyev, and D. V. Pozdnyakov, *Optical Properties and Remote Sensing of Inland and Coastal Waters* (CRC Press, 1995).
27. Z. P. Lee, http://www.ioccg.org/groups/OCAG_data.html.
28. R. Pope and E. Fry, "Absorption spectrum (380 - 700 nm) of pure waters: II. Integrating cavity measurements," Appl. Opt. **36**, 8710-8723 (1997).
29. D. Stramski., A. Bricaud, and A. Morel, "Modeling the inherent optical properties of the ocean based on the detailed composition of the planktonic community," Appl. Opt. **40**, 2929-2945 (2001).
30. M. S. Twardowski, E. Boss, J. B. Macdonald, W. Scott Pegau, A. H. Barnard and J. V. Zaneveld, "A model for estimating bulk refractive index from the optical backscattering ratio and the implications for understanding particle composition in case I and case II waters," J. Geophys. Res. **106**, 14129-14142 (2001).
31. K. J. Voss, "A spectral model of the beam attenuation coefficient in the ocean and coastal areas," Limnol. Oceanogr. **37**, 501-509 (1992).
32. C. S. Roesler and E. Boss, "Spectral beam attenuation coefficient retrieved from ocean color inversion," Geophys. Res. Lett. **30**, 1468, doi:10.1029/2002GL016185 (2003).
33. A. Morel, "Optical properties of pure water and pure sea water," in *Optical Aspects of Oceanography*, N. G. Jerlov and E. S. Nielsen, eds., (Academic, New York, 1974).
34. M. Sydor and R. A. Arnone, "Effect of suspended particulate and dissolved organic matter on remote sensing of coastal and riverine waters," Appl. Opt. **36**, 6905-6912 (1997).
35. L. Prieur and S. Sathyendranath, "An optical classification of coastal and oceanic waters based on the specific spectral absorption curves of phytoplankton pigments, dissolved organic matter, and other particulate materials," Limnol. Oceanogr. **26**, 671-689 (1981).
36. P. Gege and A. Albert, "A tool for inverse modeling of spectral measurements in deep and shallow waters" in *Remote Sensing of Aquatic Coastal Ecosystem Processes: Science and Management Applications*, L. L. Richardson and E. F. LeDrew, eds., (Springer, 2006), Chap. 4.
37. A. M. Ciotti, M. R. Lewis, and J. J. Cullen, "Assessment of the relationships between dominant cell size in natural phytoplankton communities and the spectral shape of the absorption coefficient," Limnol. Oceanogr. **47**, 404–417 (2002).
38. A. Bricaud, M. Babin, A. Morel, and H. Claustre, "Variability in the chlorophyll-specific absorption coefficients of natural phytoplankton: Analysis and parameterization," J. Geophys. Res. **100**, 13321-13332 (1995).

#87554 - $15.00 USD Received 14 Sep 2007; revised 6 Nov 2007; accepted 6 Nov 2007; published 12 Nov 2007

39. W. Hou, Z. Lee, and A. D. Weidemann, "Why does the Secchi disk disappear? An imaging perspective," Opt. Express **15**, 2791-2802 (2007).
40. D. Pozdnyakov, A. Lyaskovsky, H. Grassl and L. Petterson, "Numerical modeling of transspectral processes in natural waters: implications for remote sensing," Int. J. Remote Sens. **23**, 1581-1607 (2002).
41. J. F. Schalles, A. Gitelson, Y. Z. Yacobi, and A. E. Kroenke, "Estimation of chlorophyll a from time series measurements of high spectral resolution reflectance in an eutrophic lake," J. Phycology **34**, 383-390 (1998).
42. A. Morel and B. Gentili, "Diffuse reflectance of oceanic waters. III. Implication of bidirectionality for the remote-sensing problem," Appl. Opt. **35**, 4850-4862 (1996).
43. H. Loisel and A. Morel, "Non-isotropy of the upward radiance field in typical coastal (Case 2) waters," Int. J. Remote Sens. **22**, 275–295 (2001).

## 1. Introduction

There is a growing consensus on the need for the improvement of remotely sensed sun-induced chlorophyll fluorescence measurements for ocean color interpretation. An increasing number of applications become viable if chlorophyll fluorescence and its contribution to the NIR spectral peak near 700 nm can be measured accurately and appropriately. These include the retrieval of chlorophyll concentration [Chl] and quantum yield using current and more recently developed algorithms [1,2], detection and characterization of harmful algae blooms [3,4], improvement of [Chl] retrieval using the NIR peak [5-7], and analysis of photosynthetic processes [8].

The magnitude of sun-induced chlorophyll fluorescence is now routinely retrieved by satellite observations in the open ocean using Fluorescence Line Height (FLH) algorithms [1,4] which are broadly based on the estimation of excess reflectance at the fluorescence peak above the baseline connecting the reflectances at the wings of the fluorescence peak. In the open ocean, FLH determined in this manner usually correlates well with the actual fluorescence amplitude, with minor corrections needed depending on the choice of spectral observation bands. Unfortunately, this retrieval is much more complicated in coastal waters where chlorophyll fluorescence overlaps with a strong NIR elastic scattering peak. The overlap occurs because the confluence of strongly decreasing algal absorption and increasing water absorption, coupled in a density dependent manner with scattering by phytoplankton cell structures, is located in the same spectral region as the fluorescence emission [5, 9-11]. In addition, accurate retrievals in coastal waters are further limited because of the absence of robust atmospheric correction schemes. However, with recent advances in this area [12-14], reflectances from coastal waters can be retrieved more accurately. At the same time, multispectral reflectance data are also becoming more readily available from aircraft and satellite sensors with higher spectral resolution.

If fluorescence measurements are to be trusted in coastal waters, a more detailed analysis of the remote sensing reflectance spectra is needed to reassess existing fluorescence algorithms in order to identify sources of errors. In particular, it is important to understand their limits in coastal waters in the context of optically active constituents, including variations in specific absorption of chlorophyll and accessory pigments, CDOM absorption, and scattering and absorption by nonalgal particles (NAP). While expressions for the estimation of fluorescence magnitude are well known [2,15], there are no simple relationships that can be used to relate fluorescence magnitudes to other water constituents in coastal waters. This is one of the main reasons why the fluorescence spectral region is usually avoided in the retrieval algorithms [16]. However, if it were possible to obtain relationships which can properly connect fluorescence height to other parameters, fluorescence could then be included in the retrieval algorithms by expanding their use into the NIR.

To address these issues, this paper reconsiders the relationships between fluorescence magnitude and [Chl] in the presence of the other water constituents, some of which were previously studied [9, 17-19]. Through extensive simulations using the HYDROLIGHT radiative transfer program [20,21] special high resolution datasets appropriate to variable

#87554 - $15.00 USD Received 14 Sep 2007; revised 6 Nov 2007; accepted 6 Nov 2007; published 12 Nov 2007

coastal waters were prepared and used to reexamine existing relationships between fluorescence and water parameters, to compare them with the results of our field measurements in Chesapeake Bay as well as with field data of other authors. As part of this approach we examine the impacts of spectrally interfering effects including self absorption, CDOM and NAP absorption as well as variations in quantum yield on observed fluorescence. The results are then used to determine the range of water conditions where fluorescence plays a significant role in the NIR peak's magnitude and position, and conditions where the impacts are almost undetectable.

## 2. Methodology of field measurements

The spectral features of chlorophyll *a* fluorescence are well known [15] with a peak centered at approximately 685 nm. These features are usually approximated by a Gaussian shape with a full width at half maximum (FWHM) of 25 nm [4]. This description is commonly included in simulation models [4] and in the algorithms for fluorescence retrieval [1]. At the same time, it is also known [15] that fluorescence overlaps with major changes in the chlorophyll absorption spectrum. For example, the *in vivo* chlorophyll *a* specific absorption coefficients decrease from 0.0203 $m^2$/ mg at 674 nm, to 0.0076 at 686 m, to 0.0008 at 700 nm [22]. Several approaches were used to disentangle the overlapping spectral features of chlorophyll fluorescence and the elastic NIR peak. These include long pass and band pass filter methods [9, 23], polarization discrimination [10,11] and comparison of measured total reflectance with the simulated elastic reflectance based on retrieved inherent optical properties (IOP) [19]. It was shown in the laboratory tests and in the field that fluorescence can contribute from about 4% [9] to 30% [11, 23] to the magnitude of the reflectance peak in the NIR, thereby affecting retrieval algorithms considerably. In our methodology, we used an approach similar to [19] to estimate fluorescence reflectance components, however, instead of using retrieved IOPs, we utilized measured spectra from our WET Labs sensor package (see more detailed description below).

In-situ measurements were carried out at 42 stations over the Maryland coast of the Chesapeake Bay and adjacent rivers and harbors during July 11-20, 2005. The upwelling water radiance $L_u(\lambda)$ was collected using a fiber optic probe placed just beneath the water surface and connected to USB2000 Ocean Optics spectrometer. Another probe with a cosine collector connected to a similar spectrometer was used to collect downwelling irradiance $E_d(\lambda)$. Both spectrometers had undergone absolute radiometric calibration before the cruise. (See [7] for descriptions of the study area, paired upwelling and downwelling measurements, and laboratory procedures for water analysis). Remote sensing reflectance below the surface $r_{rs}(\lambda)$ was obtained from normalization of the upwelling radiance, $L_u(\lambda)$, to the downwelling irradiance, $E_d(0+)$ multiplied by air-water transmission which was assumed to be 0.96:

$$r_{rs}(\lambda) = L_u(\lambda) / E_d(\lambda). \quad (1)$$

The $L_u(\lambda)$ values were also measured in parallel using a GER spectroradiometer with a fiber optic probe and were normalized to the downwelling irradiance $E_d(\lambda)$ measured by the same probe from a Spectralon plate. The data from both measurement sets were checked and found to show very similar reflectance spectra.

Water samples were also collected at each station. From these [Chl] concentrations were obtained using filtration through glass fiber filters (Whatman GFC) within several hours of sample collection, freezing of filters for at least 24 h, extraction with grinding in 90% buffered acetone, and spectrometric determination with a Genesis 2 spectroradiometer (Spectronics Corp.) and the trichromatic equation for total chlorophyll *a* [24]. CDOM was

#87554 - $15.00 USD Received 14 Sep 2007; revised 6 Nov 2007; accepted 6 Nov 2007; published 12 Nov 2007

estimated from absorption measurement of the sample filtrate and total suspended solids (TSS) concentrations were determined gravimetrically with tared, pre-ashed glass fiber filters.

Water IOP parameters at sample sites were measured using a ship-deployed profiling package assembled by WET Labs (Philomath, Oregon). This package consisted of three instruments: an AC-S recording total absorption (a) and total attenuation (c) at 82 wavelengths almost equally spaced between 400 nm and 750 nm giving an average spectral resolution of 4 nm, an ECO-scattering meter with one of the channels measuring the fluorescence signal of chlorophyll, and a CTD to obtain temperature, salinity and pressure data. The AC-S instrument was properly calibrated using optically pure water as a reference (Barnstead NANOpure) before and after the cruise in order to track and compensate for any drift. The AC-S data were corrected for temperature, salinity and scattering according to the manufacturer recommendations. A data logger was used to power all the instruments, acquire data, coordinate different timing schemes and transmit the data up through a single cable to the processing computer. The depth of the WET Labs profiler package was raised and lowered either manually or by automatic winch in order to sample depth profiles. The range of parameters measured in the field was [Chl] = 9.1 -354.2 mg/m$^3$, total absorption at 400 nm 1.41 -10.8 m$^{-1}$, concentrations of total suspended solids TSS 7 – 64.8 g/m$^3$ demonstrating a wide variability of conditions.

### 3. Synthetic datasets and relationships for the bio-optical model

To analyze the relationships of fluorescence with other water parameters a four-component bio-optical model was used to generate the IOPs of the water body [25,26]. This model provided inputs for HYDROLIGHT program which was then used to generate a series of reflectance spectra datasets. The constituents included: the water itself, yellow substance (CDOM), nonalgal particulates - mineral and detritus (NAP) and chlorophyll containing particles (phytoplankton). We use the subscripts “w”, “y”, “nap” and “chl” to identify these four components in the text below. Our simulations closely followed assumptions used in the simulations of the of IOCCG database [27] but with several significant differences. First, for accurate fluorescence evaluation and retrieval, datasets were simulated from 400 to 800 nm with 1 nm resolution instead of 10 nm. Secondly, concentrations of CDOM and NAP were assumed to be random and not related to [Chl] as necessary for case 2 water conditions. The main model relationships are explained below.

The total spectral absorption coefficient $a(\lambda)$ is given as

$$a(\lambda) = a_w(\lambda) + a_y(\lambda) + a_{chl}(\lambda) + a_{nap}(\lambda), \tag{2}$$

where the water absorption spectrum $a_w(\lambda)$ was obtained from Pope and Fry [28].

The chlorophyll absorption for case 2 (coastal) waters was considered proportional to [Chl] as is often assumed [21] and given by:

$$a_{chl}(\lambda) = [Chl] \cdot a^*_{chl}(\lambda), \tag{3}$$

where $a^*_{chl}(\lambda)$ is the specific chlorophyll absorption spectrum, m$^2$/mg. The choice of the specific chlorophyll absorption spectra is critical to the corresponding reflectance spectra and fluorescence magnitudes and is discussed below in more detail.

The absorption spectra of both NAP and CDOM were both modeled as having exponentially decreasing magnitudes with wavelength and determined from their base reference values at 400 nm as in [26, 29]:

$$a_{nap}(\lambda) = a_{nap}(400) \cdot \exp(-S_{nap}(\lambda - 400)), \tag{4a}$$

$$a_{nap}(400) = C_{nap} \cdot a^*_{nap}(400), \tag{4b}$$

#87554 - $15.00 USD Received 14 Sep 2007; revised 6 Nov 2007; accepted 6 Nov 2007; published 12 Nov 2007

where $a^*_{nap}(400)$ is the specific absorption of nonalgal particulates at 400 nm, $m^2/(g)$ and $C_{nap}$ is a concentration, $g/m^3$.

CDOM absorption was obtained from the relationship:

$$a_y = a_y(400)\exp(-S_y(\lambda - 400)), \tag{5}$$

where $a_y(400)$ is the absorption of CDOM at 400 nm, $m^{-1}$.

Ranges of parameters for the datasets were taken as:

$$a^*_{nap} = 0.02 - 0.1 m^2/g,\ S_y = 0.01 - 0.02,\quad S_{nap} = 0.007 - 0.015.$$

The total scattering coefficient was simulated as a sum of three components:

$$b(\lambda) = b_w(\lambda) + b_{chl}(\lambda) + b_{nap}(\lambda), \tag{6}$$

where $b(\lambda)$ is the total scattering coefficient, $m^{-1}$. Here, the scattering of NAP was assumed to be modeled by a power law function [29, 30] as follows:

$$b_{nap}(\lambda) = b_{nap}(550)(\frac{550}{\lambda})^{\gamma_2}, \tag{7a}$$

$$b_{nap}(550) = b^*_{nap}(550)\cdot C_{nap}, \tag{7b}$$

where $b^*_{nap}(550)$ is a specific scattering of non algal particles at 550 nm, $m^2/g$.

The ranges of parameters for scattering were:

$$\gamma_2 = 0.5 - 2 \qquad b^*_{nap}(550) = 0.5 - 1\ m^2/g.$$

To model the scattering of phytoplankton, both Mie calculations and field measurements indicate that the scattering spectrum of algae cells can be calculated as the difference between their attenuation and absorption [31, 32],

$$b_{chl}(\lambda) = c_{chl}(\lambda) - a_{chl}(\lambda), \tag{8}$$

while the attenuation spectrum itself can be modeled as a power law function [31]:

$$c_{chl}(\lambda) = c_{chl}(550)(\frac{550}{\lambda})^{\gamma_1} \tag{9a}$$

and

$$c_{chl}(550) = p\ [Chl]^{0.62}, \tag{9b}$$

where $p = 0.1 - 0.5$ and $\gamma_1 = 0.1 - 1.6$.

In our simulations, the backscattering coefficient was taken to be the sum of the contributing components

$$b_b(\lambda) = b_{bw}(\lambda) + \tilde{b}_{b\,chl} * b_{chl}(\lambda) + \tilde{b}_{bnap} * b_{nap}(\lambda), \tag{10}$$

where $b_{bw}(\lambda)$ is obtained according to [33] and $\tilde{b}_{b\,chl}$, $\tilde{b}_{bnap}$ are backscattering ratios for chlorophyllous and nonalgal particles assumed to be independent of wavelength [30, 34]; typical values were used $\tilde{b}_{b\,chl} = 0.01$ and $\tilde{b}_{b\,nap} = 0.02$ (assuming a strong mineral component in NAP) together with the predefined Fournier-Forand phase function.

#87554 - $15.00 USD Received 14 Sep 2007; revised 6 Nov 2007; accepted 6 Nov 2007; published 12 Nov 2007

The bio-optical model for the simulation of IOP spectra described above uses 3 main parameters as inputs: the concentration of phytoplankton [Chl], the concentration of nonalgal particles $C_{nap}$, and the absorption of CDOM at 400 nm $a_y(400)$. To generate HYDROLIGHT datasets, values of all constituents were randomly varied within the prescribed ranges identified for each dataset. Simulations were divided into 2 datasets, each representative of different ranges of nonalgal particle content.

Dataset 1: 500 runs were executed with randomly chosen values: [Chl] = 1-100 mg/m$^3$, $C_{nap}$ = 0 – 1 g/m$^3$ and $a_y(400)$ = 0 – 5 m$^{-1}$. With a wide variety of specific chlorophyll absorption spectra available [35-38] in our case the set of specific absorptions was taken from Ciotti et al. [37] as a sum of specific absorptions of microplankton and picoplankton with different weighting factors, $S_f$ ,where $S_f = [0.1,0.2,0.3,0.4,0.5]$.

$$a^*_{chl}(\lambda) = S_f \cdot a^*_{pico}(\lambda) + (1 - S_f) \cdot a^*_{micro}(\lambda) \tag{11}$$

These spectra are shown in Fig. 1. They assume similar spectral shape and relatively low specific absorption amplitudes which are typical for waters with [Chl] > 1-5 mg/m$^3$ [38] ($a_{chl}(675)$ = 0.01 – 0.016). Higher values 0.5 < $S_f$ < 1 correspond to the specific absorption spectra more typical for open ocean waters with lower [Chl] and were not considered in this study.

Dataset 2 follows dataset 1, but with nonalgal particle concentrations in the range $C_{nap}$ = 1 – 100 g/m$^3$.

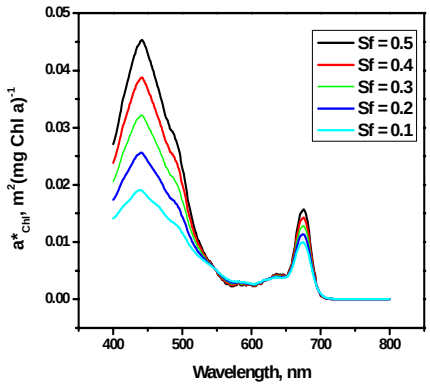


Fig. 1. Specific chlorophyll absorption spectra used in simulations.

Datasets of reflectances were calculated both with and without fluorescence and assuming a fluorescence quantum yield of $\eta_0$ = 1%. All reflectances were simulated for the sun zenith angle $\theta_i$ = 30° and for nadir observation. The solar input was simulated using the Gregg and Carder model with a cloud-free sky [20,21] and the default wind speed was 5 m/s. Since the final fluorescence signal is completely linear with the value of $\eta_0$, it can be scaled accordingly as needed. Finally, the water body was assumed homogeneous with a maximum integration depth specified as $z_{\max} = 5/c(685)$ (where c(685) is the attenuation at 685 nm) to account for the deepest layer which can contribute to the fluorescence detected at the surface [39].

#87554 - $15.00 USD Received 14 Sep 2007; revised 6 Nov 2007; accepted 6 Nov 2007; published 12 Nov 2007

## 4. Relationships between fluorescence amplitude and concentrations of chlorophyll and other water constituents – simulations and measurements

### *4.1 Basic features of the relationship*

The amplitude of the fluorescence peak in the water leaving radiance at 685 nm can be derived following Huot, *et al*. [2] as:

$$Fl = \frac{1}{4\pi} \cdot \frac{\eta}{C_f} \cdot Q_a^* \cdot [Chl] \cdot \int_{400}^{700} (a_{Chl}^*(\lambda) \cdot E_d(\lambda,0)/(K(\lambda)+K_f)) \cdot d\lambda \tag{12}$$

where $Q_a^*$ is a reabsorption coefficient in the algae cells, $E_d(\lambda,0)$ is the downwelling irradiance just below the surface, η is the fluorescence quantum yield, $K(\lambda)$ is the attenuation coefficient in the fluorescence excitation zone, $K_f$ is the attenuation coefficient in the fluorescence emission zone, $C_f$ is a coefficient which depends on the assumed fluorescence shape and which also takes into account propagation of the fluorescence through the air-water interface. The integral in (12) clearly shows the modification of photosynthetically available radiation (PAR) due to absorption and scattering in the water.

According to Babin et al. [15] $Q_a^*$ = 0.3 – 0.6 for [Chl] > 1 mg/m$^3$. To take reabsorption into account in HYDROLIGHT simulations and make it consistent with (12), we assumed a value of $Q_a^*$ =0.5. Since $Q_a^*$ value is not included directly in the HYDROLIGHT program we scaled the fluorescence quantum yield as $\eta = \eta_0 / Q_a^*$ (i.e. by a factor of 2).

In algae dominated waters, the amplitude of fluorescence component in water leaving radiance in radiance units (Wm$^{-2}$sr$^{-1}$μm$^{-1}$) for vertical illumination and detection is determined by [Chl], absorption of water $a_w(\lambda)$ and specific absorption of algae $a_{Chl}^*(\lambda)$. In fact, it is useful for parameterization purposes to use a the simplified version [18] of expression (12) with attenuation terms in the integral replaced by the sums of average absorption values in the excitation and emission zones

$$Fl = 0.15[Chl]\{a_{wsum}/(a_{wsum} + a_{Chl\,sum}^*[Chl])\}. \tag{13}$$

Here, $a_{wsum} = a_w^{ex} + a_w^{em}$, $a_{Chl\,sum}^* = a_{Chl}^{*ex} + a_{Chl}^{*em}$, $a_w^{ex}$ is the average absorption of water in the excitation wavelength region 400-700 nm, $a_w^{em}$ is the average absorption of water in the emission wavelength region around 685 nm and $a_{Chl}^{*ex}$ and $a_{Chl}^{*em}$ are algae specific absorptions in the excitation and emission zones with all other parameters included in the proportionality coefficient. Summing the absorptions is required since the downwelling light is attenuated by absorption in the excitation band while upwelling fluorescence is similarly attenuated in the emission band.

The coefficient in the expression (13) implicitly includes specific chlorophyll absorption in the excitation zone $a_{Chl}^{*ex}$ and will change proportionally to its value. This coefficient was chosen [18] to be consistent with the relationship $Fl = 0.15[Chl]$ which is obtained from field measurements for very clear waters with low [Chl] where the only attenuation factor is water absorption. In waters with higher [Chl] attenuation by phytoplankton absorption should be taken into account by adding the $a_{wsum}/(a_{wsum} + a_{Chl\,sum}^*[Chl]$ term. Estimation of

#87554 - $15.00 USD Received 14 Sep 2007; revised 6 Nov 2007; accepted 6 Nov 2007; published 12 Nov 2007

$a_{wsum}$ and $a^{*}_{Chl\ sum}$ in the excitation and emission zones, results in the following parameterized formula for the fluorescence amplitude suitable for open ocean [18]

$$Fl = 0.15[Chl]/(1 + 0.2\,[Chl]). \tag{14}$$

Here, the fluorescence amplitude at 685 nm is expressed in radiance units ($Wm^{-2}sr^{-1}\mu m^{-1}$), the coefficient 0.2 in the denominator has units of $m^3/mg$ $(a^{*}_{Chl\ sum} / a_{w\,sum})$ as needed to make the denominator non-dimensional and coefficient 0.15 has units of radiance per [Chl] $(Wm^{-2}sr^{-1}\mu m^{-1})^{*}$ $(m^3/mg)$.

With increasing [Chl] concentrations, saturation occurs because of stronger light absorption in both excitation and fluorescence emission zones. For non-nadir illumination angles, the absorption in both emission and excitation bands needs to be multiplied by $\mu_i = 1/\cos\vartheta_i$, and $\mu_v = 1/\cos\vartheta_v$ respectively, where $\vartheta_i$ and $\vartheta_v$ are the related illumination and viewing angles. Since absorption of water in the excitation band is small in comparison with the emission band, variations due to illumination angle in the range 0 – 30° are noticeable only for high [Chl]. Coefficients in (14) are based on case 1 waters assumptions, in particular high specific chlorophyll absorption. With increasing [Chl] these values become lower [38] and coefficients should be changed, so Eq. (14) will be less and less accurate.

Since Eq. (14) is based on experimental data it is useful to estimate fluorescence quantum yield in this expression. Remote sensing reflectances above water were simulated (independently of datasets 1 and 2) using HYDROLIGHT and standard case 1 water assumptions with and without fluorescence and $\vartheta_i$ = 30°. The subtraction of these two spectra at 685 nm defined the simulated fluorescence amplitude. When a fluorescence quantum yield of $\eta$ = 1% is used in the simulations, the amplitude of the simulated fluorescence (at 685 nm) agrees very well with the amplitude obtained from Eq. (14) for [Chl] = 1 – 15 $mg/m^3$ (Fig. 2).

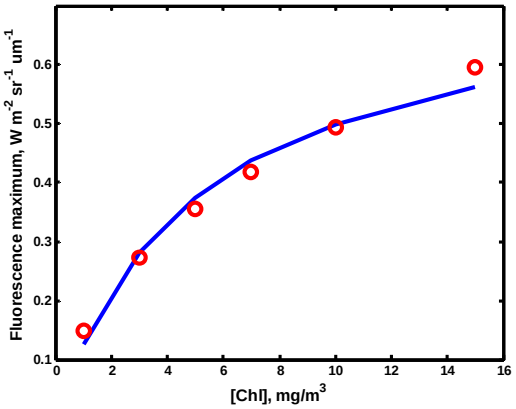


Fig. 2. HYDROLIGHT simulation (o) and calculated fluorescence amplitude from equation (14) (solid line) for case 1 waters.

This very good agreement provides a very strong constraint on the quantum efficiency and motivates us to explore this question further for case 2 waters.

We should note that in order to obtain the simulated fluorescence value in radiance units ($Wm^{-2}sr^{-1}nm^{-1}$) compatible with Eq. (14), we multiplied here and throughout the paper the fluorescence amplitude obtained as an equivalent remote sensing reflectance by the irradiance at 685 nm ($E_d$ = 1.1 $Wm^{-2}$ $nm^{-1}$), which is calculated in HYDROLIGHT for clear sky conditions just above the surface and $\vartheta_i$ = 30°.

#87554 - $15.00 USD Received 14 Sep 2007; revised 6 Nov 2007; accepted 6 Nov 2007; published 12 Nov 2007

The simple model (13-14) described above does not correspond to case 2 waters. In coastal waters, with the presence of CDOM and mineral particles, attenuation is not limited to the absorption by phytoplankton, as in the open ocean, but should also include absorption of CDOM and NAP as well as NAP backscattering. So the relationship between Fl and [Chl] should take into account these attenuation components. Thus, if these components are now included in the development of Eq. (13) as additional attenuation mechanisms we get

$$Fl \sim [Chl]\{a_{w\,sum}/(a_{CDOM\ sum}+a_{nap\ sum}+b_{b\ nap\ sum}+a^{*}_{Chl\ sum}\,[Chl])\}, \qquad (15)$$

or

$$Fl \sim [Chl]/\{1+(a_{CDOM\ sum}+a_{nap\ sum}+b_{b\ nap\ sum}+a^{*}_{Chl\ sum}\,[Chl])/a_{w\,sum}\}, \qquad (16)$$

where $a_{w\,sum} \approx 0.5$ m$^{-1}$ [18] and $a_{CDOM\,sum}$, $a_{nap\,sum}$ and $b_{b\,nap\,sum}$ are respectively the sums of CDOM, NAP absorptions and backscattering of nonalgal particles in the excitation and emission spectral regions. Since CDOM, NAP absorptions and backscattering decrease rapidly with wavelength (Eqs (4), (5) and (7)) they can be generally neglected in the emission band as a first approximation. In addition, for the low NAP case, the impact of backscattering can be also considered substantially smaller than that of absorption.

All terms on the right side of Eq. (16) can be calculated from the relationships in Section 3 for the given input parameters [Chl], $a_y(400)$ and $C_{nap}$ which also provide the IOPs needed for the simulations. The fluorescence amplitudes can be taken from reflectance simulations (with and without fluorescence), thus establishing proportionality coefficient for (16). Unfortunately this approach does not provide an absolute proportionality constant because of the unknown fluorescence quantum yield. Recourse to field measurements is needed to address this question.

*4.2 Determination of Quantum Efficiency Parameter Regime*

Unlike case 1, waters in coastal waters field data are generally sparse, and simultaneous measurements of water leaving reflectance, water IOPs and chlorophyll concentrations are not readily available. Therefore, it is much harder to relate the model to measurements. However, a significant increase in experimental validation would result if we can connect the quantum yield directly to the water leaving reflectance properties without complementary measurements of IOPs, since there are more measurements of this type available in case 2 waters. In this section, we show how quantum yield can be related to features in the reflectance spectra, which result in strong constraints on the fluorescence quantum yield.

Thus, while generally, it is assumed that the fluorescence quantum yield can vary widely, in a range of 0.3% to 10% [17, 19, 40], we will show below, that the observed variability is usually much less. If this were not the case, it would lead to appearance of reflectance features in the NIR, which are not, in fact observed in the field.

As discussed in the introduction, the NIR peak in the reflectance spectra is a sum of the overlapping spectra of fluorescence and elastic reflectance. The elastic reflectance spectrum itself is a result of the confluence of the decreasing algal absorption and increasing absorption of water which creates a local minimum on the total absorption spectrum that therefore corresponds to the maximum on the reflectance spectrum. As shown in Fig. 3 for low [Chl] < 6 mg/m$^3$, the fluorescence component is a dominant part of the NIR peak and the maximum of the reflectance is close to the position of the fluorescence maximum at 685 nm. With an increase in [Chl], the elastic peak becomes stronger and shifts to the red, causing the combined fluorescence/elastic reflectance peak to shift in the same direction. For high [Chl] > 60 – 70 mg/m$^3$ elastic part of the peak is dominant and significantly less dependent on the fluorescence component. In fact, it was found in [41] that the shift of the total NIR peak from 685 nm is clearly related to [Chl] as shown in Fig. 4.

#87554 - $15.00 USD Received 14 Sep 2007; revised 6 Nov 2007; accepted 6 Nov 2007; published 12 Nov 2007

These data are complemented by our Chesapeake Bay field measurements results of which encompass a broader range of conditions. For Chesapeake Bay data the upper boundary is similar to results obtained in [41] which were approximated by us in Fig. 4 (solid line). The lower boundary for Chesapeake data was also approximated (dashed line) for [Chl] < 100 mg/m$^3$. (The older data [41] were measured in a hypereutrophic oxbow lake with spring diatom and summer and fall cyanobacteria blooms.)

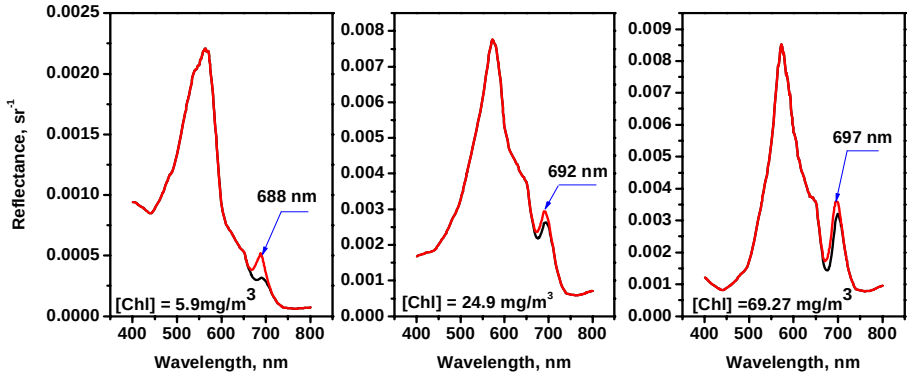


Fig. 3. Shift of NIR maximum and changes in reflectance spectra with [Chl]: red – total reflectance spectra, black – elastic spectra.

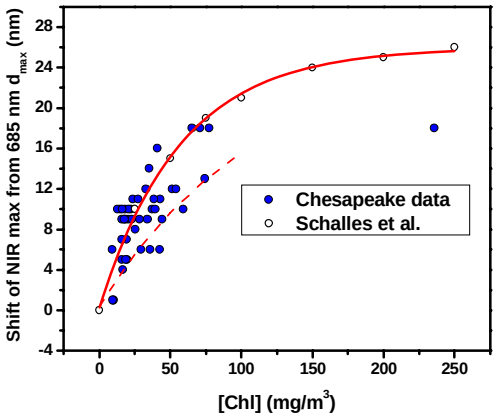


Fig. 4. Shift of NIR maximum with [Chl]. The solid line is a fitted approximation of data from Schalles et al. [41], dashed line – approximation of the lower boundary for Chesapeake data and [Chl] < 100 mg/m$^3$.

These results, in fact, impose significant limitations on the fluorescence amplitude values which can be assumed in modeling. If the fluorescence is too dominant for a given [Chl] level, the shifts in the NIR reflectance peak from the fluorescence peak at 685 nm will be much less than those observed in the field, while if the fluorescence is much less, deviations would be larger than observed in the field. This is borne out by comparison with the results of simulations in Fig. 5, where shifts of the reflectance peak in the NIR (similar to the one shown in Fig. 4) were simulated for reflectances from dataset 1 with an absorption shape corresponding to $S_f$ = 0.5 (see Fig. 1) and three fluorescence quantum yield values $\eta$ = 0, 1 and 2 %. These results are then compared with the field data from Fig. 4.

#87554 - $15.00 USD Received 14 Sep 2007; revised 6 Nov 2007; accepted 6 Nov 2007; published 12 Nov 2007

In general, the spectral shifts obtained from our field data fall between the boundary conditions (dash curves in Fig. 5) and are consistent with the shifts observed from our HYDROLIGHT simulation for $\eta$ = 1%. For other specific chlorophyll absorption shapes $S_f$ < 0.5 (Fig. 1), the results were similar or corresponded to slightly lower quantum efficiency. Based on these results, we assume $\eta$ = 1% in the following analysis. This value is the same as for case 1 waters as suggested by Babin et al. [15] and also follows from our previous case I results in Section 4.1.

Further analysis of Fig. 5 shows that for [Chl] > 60 – 70 mg/m$^3$ fluorescence does not significantly affect the NIR peak (blue, green and red points corresponding to $\eta$ = 0, 1 and 2% are very close to each other).

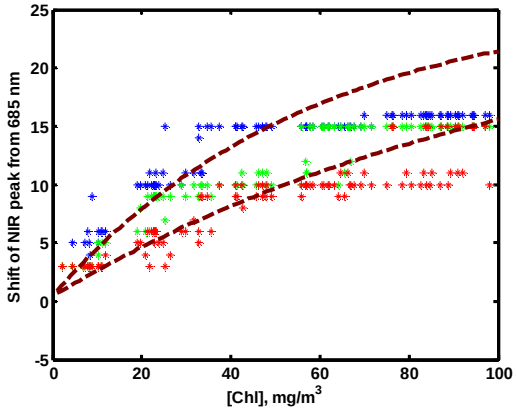


Fig. 5. Shift of NIR maximum on reflectance spectra with [Chl] based on simulated data from dataset 1 ($S_f$ = 0.5) for η = 0 – blue, 1% – green, 2% – red. Dashed lines are upper and lower boundaries of data in Fig. 4.

*4.3 Refinement of relations between fluorescence amplitude and concentrations of water constituents from simulated datasets*

Using our simulations, which generated reflectance spectra with and without fluorescence and using the fluorescence quantum yield value determined above, we calculated fluorescence amplitudes at 685 nm for our datasets and extended the original expression in Eq. (14) in accordance with the approach followed to derive expression (16). Applying $\eta$ = 1% to the datasets 1 ($C_{nap}$ < 1 g/m$^3$) and 2 ($C_{nap}$ = 1-100 g/m$^3$), we found the best LSQ fit for the relation

$$Fl = x1*[Chl]/(1+x2*a_y(400)+x3*C_{nap}+x4*[Chl]), \qquad (17)$$

where the term $x2*a_y(400)$ accounts for the effect of CDOM and the term $x3*C_{nap}$ for the effect of nonalgal particles.

For dataset 1, we find that the effect of nonalgal particles is negligible and the relation takes the form

$$Fl = 0.0375[Chl]/(1+0.32\,a_y(400)+0.032\,[Chl]), \qquad (18a)$$

In this expression the coefficient in the numerator is reduced from 0.15 in (14) to 0.0375, and the coefficient 0.2 at [Chl] in the denominator is reduced to 0.032, which is due to the lower

#87554 - $15.00 USD Received 14 Sep 2007; revised 6 Nov 2007; accepted 6 Nov 2007; published 12 Nov 2007

specific chlorophyll absorption in coastal waters for high [Chl] compared with the specific absorption model for open ocean waters [38]. Lower specific chlorophyll absorptions mean smaller PAR which results in the smaller coefficient in the numerator and smaller $a^*_{Chl\ sum}$ values in (16). This relationship is illustrated in Fig. 6(a) which shows that in the low NAP case, expression (18a) can be successfully used to quantify fluorescence amplitude with a correlation coefficient $R^2$ = 0.938 where the fluorescence is explicitly connected to the CDOM absorption and [Chl]. In addition, we found that the variability of specific chlorophyll absorptions (Fig. 1) does not significantly affect the correlation.

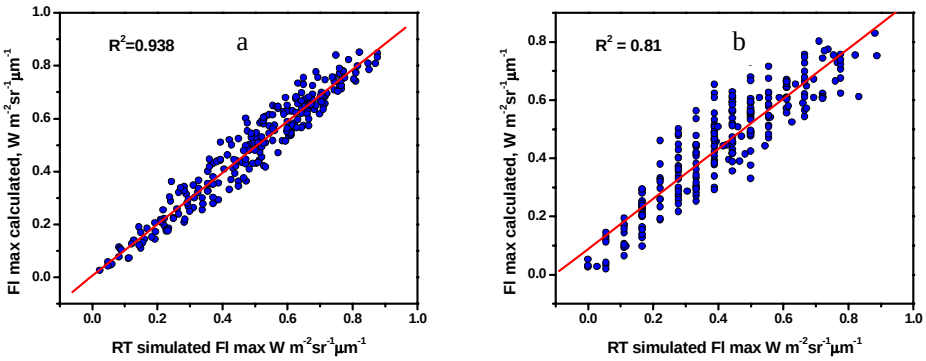


Fig. 6. Comparison of fluorescence amplitudes: a) calculated from (18a) and simulated using the HYDROLIGHT radiative transfer (RT) program for low nonalgal particle conditions $C_{nap}$ < 1 g/m$^3$, b) calculated from (18b) and simulated using HYDROLIGHT for high nonalgal particle conditions $C_{nap}$ = 1 - 100 g/m$^3$.

Taking into account the concentration of nonalgal particles and using dataset 2 we arrive at Eq. (18b).

$$Fl = 0.0375[Chl]/(1 + 0.32\, a_y(400) + 0.01 C_{nap} + 0.032\,[Chl]) \qquad (18b)$$

We note that the correlation is somewhat lower ($R^2$ = 0.81) for the high NAP case if expression (18b) is used to calculate fluorescence (Fig. 6(b)). However, this reflects not only the variability of the specific scattering of non-algal particles $b^*_{nap}(550)$ and scattering spectra slope $\gamma_2$ (see description in Section 3 for details) but also the changes in the fluorescence spatial distribution in the presence of a highly scattering medium. Our simulations showed that this correlation significantly improves if $C_{nap}$ is limited to 10 g/m$^3$ but even for the whole range of $C_{nap}$ = 1 – 100 g/m$^3$, we consider this expression to be a good first approximation of the fluorescence amplitude for waters where both CDOM and nonalgal particles contribute to the attenuation of light.

Thus, the relationships (18a,b) estimate fluorescence amplitude as a function of [Chl], absorption of CDOM $a_y(400)$ and concentration of nonalgal particles $C_{nap}$. If all three of these parameters are known, estimation of fluorescence amplitude $Fl$ is straightforward. However, it is not likely that the field data in many cases will be sufficiently accurate for point by point comparison of $Fl$ due to the inherent measurement inaccuracies as well as the complexity of coastal waters. But the model can be also used in a statistical way to define a confidence region in the $Fl$ - [Chl] plane where we can expect the bulk of the measurements

#87554 - $15.00 USD Received 14 Sep 2007; revised 6 Nov 2007; accepted 6 Nov 2007; published 12 Nov 2007

to occur and where the boundaries of these regions are formed by taking appropriate limits, as follows.

*4.3.1 Low NAP concentration with varying CDOM absorption*

From Eq. (18a) we find that for the average CDOM absorption in dataset 1 $a_y(400)$ =2.5 $m^{-1}$ in the absence of nonalgal particles $Fl$ is given by:

$$Fl = 0.0375[Chl]/(1 + 0.8 + 0.032\,[Chl]), \tag{19a}$$

in the absence of CDOM, $a_y(400) = 0$ which establishes the higher boundary for $Fl$ as

$$Fl = 0.0375[Chl]/(1 + 0.032\,[Chl]) \tag{19b}$$

and for maximum CDOM, $a_y(400)$ = 5 $m^{-1}$ which establishes the lower $Fl$ boundary as

$$Fl = 0.0375[Chl]/(1 + 1.6 + 0.032\,[Chl]). \tag{19c}$$

4.3.2 High NAP concentration

From dataset 2 with $C_{nap}$ =1- 100 g/$m^3$ we find the lower $Fl$ boundary which occurs when both $a_y(400)$ and $C_{nap}$ are near their maximum and is given by:

$$Fl = 0.0375[Chl]/(1 + 4.0 + 0.032\,[Chl]). \tag{19d}$$

The value 4.0 in the denominator is higher than the value which can be calculated from the full expression (18b) directly. This reflects the errors in (18b) for high $C_{nap}$ .

The complete set of expressions (19a-d) together with expression (14) can be utilized to determine realistic bounds of $Fl$ over case 1 and case 2 waters.

*4.4 Comparison and assessment of models for fluorescence values*

*4.4.1 Models derived from radiative transfer simulations*

Relationships (19a-d) for coastal waters together with relationship (14) for the open ocean waters are shown in Fig. 7. As discussed earlier, the assumptions for the open ocean become less accurate with increasing [Chl], so the curve 1 in Fig. 7 only applies to conditions where [Chl] < 20 mg/$m^3$.

The main conclusion from Fig. 7 is that the fluorescence amplitude is usually lower in case 2 waters than in the open ocean because of the smaller specific chlorophyll absorption values, attenuation of light in the excitation and emission spectral zones by absorption of CDOM and/or NAPs and NAP backscattering, thus making detection of fluorescence much more challenging. As there is no exact boundary between case 1 and case 2 waters, the zone between curves 1 and 3 will correspond to conditions close to case 1 waters, but with higher CDOM values, as well as to the waters with higher specific chlorophyll absorptions which can be modeled with the values of $S_f$ > 0.5 in (11) which are more typical for open ocean waters. Finally, we should comment that at very high [Chl], the curves in Fig. 7 have some saturation levels which depend on concentrations of CDOM and nonalgal particles but these conditions correspond to very strong algae blooms which should be considered separately and are beyond the scope of this paper.

#87554 - $15.00 USD Received 14 Sep 2007; revised 6 Nov 2007; accepted 6 Nov 2007; published 12 Nov 2007

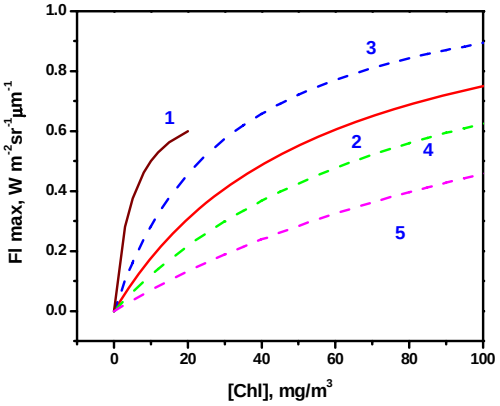


Fig. 7. Comparison of fluorescence amplidudes calculated from (14) and (19) as a function of [Chl] for various conditions: 1 – Case 1 waters (14); 2 - Case 2 waters, low NAP case, average CDOM absorption (19a); 3 and 4 – Case 2 waters, upper and lower Fl boundary for low NAP case (19b,c); 5 – Case 2 waters, lower Fl boundary for high NAP case (19d).

*4.4.2 Comparison with field measurements*

To test the above simulation results on field data, we modeled the total below surface reflectance spectrum for each station as a sum of two components. The first component was the elastic reflectance spectrum as calculated from measured attenuation and absorption spectra using the WET Labs AC-S instrument, and the second was a fluorescence reflectance component. These are derived as shown below using Eq (20).

$$r_{rs\,\mathrm{mod}}(\lambda) = \frac{(0.37/Q) * \tilde{b}_{b\,\mathrm{mod}}\; b_m(\lambda)}{a_m(\lambda) + \tilde{b}_{b\,\mathrm{mod}}\; b_m(\lambda)} + r_{fl\,\mathrm{mod}} * \Phi(\lambda), \tag{20}$$

Here, $r_{fl\,\mathrm{mod}}$ is the fluorescence amplitude in remote sensing reflectance below the surface, and $\Phi(\lambda)$ is the fluorescence spectral distribution, which was considered Gaussian with a peak at 685 nm and 25 nm FWHM and $Q$ is the bidirectional factor with a value of $Q$ = 4.5. $b_m(\lambda)$ and $a_m(\lambda)$ are the field determined scattering, and absorption spectra. The scattering is not obtained directly but is deduced from $b_m(\lambda) = [c_m(\lambda) - a_m(\lambda)]$, where $c_m(\lambda)$ is the measured attenuation coefficient.

This total reflectance has two free parameters $\tilde{b}_{b\,\mathrm{mod}}$ and $r_{fl\,\mathrm{mod}}$. We retrieved the fluorescence component $r_{fl\,\mathrm{mod}}$ by fitting modeled reflectance $r_{rs\,\mathrm{mod}}(\lambda)$ into the measured below surface reflectance spectrum with values of $\tilde{b}_{b\,\mathrm{mod}}$ and $r_{fl\,\mathrm{mod}}$ determined with LSQ approach. In practice, model parameters were found based on constrained LSQ minimization with the boundaries for $\tilde{b}_{b\,\mathrm{mod}}$ taken as 0.005 to 0.4 and $r_{fl\,\mathrm{mod}}$ taken to vary from 0 to 0.1 which includes almost all realistically possible variations of these parameters. To compare fluorescence amplitudes with our previous simulation results from datasets 1 and

#87554 - $15.00 USD Received 14 Sep 2007; revised 6 Nov 2007; accepted 6 Nov 2007; published 12 Nov 2007

2, we assumed that the fluorescence amplitude is given by $Fl_{field} = 0.53 r_{fl\,\mathrm{mod}} E_d$, where $E_d$ =1.1 $Wm^{-2}$ $nm^{-1}$ is the downwelling irradiance in the fluorescence zone, (the same value as was used in the simulation analysis) and where the 0.53 factor accounts for the reflectance ratio at the water – air interface [42].

Out of 42 stations for which both reflectance and WET Labs data were available, the fluorescence was retrieved for 28 stations. For other stations, attenuation spectra could not be measured completely because of saturation in some parts of the spectra or because there was an obvious mismatch between simulated and measured spectra, probably due to the local changes in the water composition at the sites where reflectance and WET Labs data were acquired.

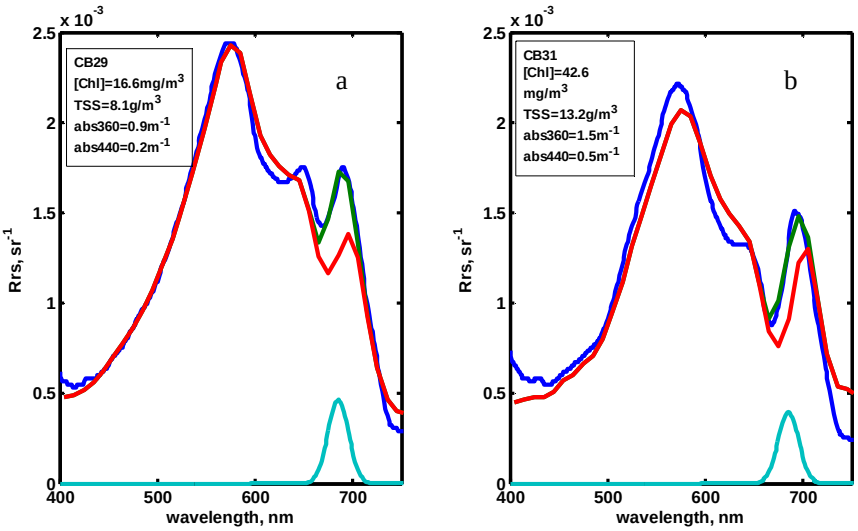


Fig. 8. HYDROLIGHT simulated from WET Labs data and retrieved fluorescence amplitude; a – lower [Chl], b - higher [Chl]. Red – simulations of elastic reflectance, blue – measured reflectance, green- fit with fluorescence, cyan – fluorescence.

Typical total measured and modeled reflectance spectra, modeled elastic spectra and retrieved fluorescence spectra are shown in Figs. 8(a) and 8(b) for 2 stations. These stations had significant differences in [Chl], but other parameters were more uniform. Total suspended solids (TSS) were 8.1 and 13.2 $g/m^3$, $a_y(400)$ was about 0.55 $m^{-1}$ and 1.0 $m^{-1}$, and [Chl] was 16.6 $mg/m^3$ and 42.6 $mg/m^3$ respectively. In both cases, the fluorescence was a significant part of the NIR peak. However, for [Chl] = 46.6 $mg/m^3$, a larger proportion of the peak was due to elastic reflectance and absorption changes, and the cumulative NIR peak location was at a significantly longer wavelength than the fluorescence peak. It is important to remember that TSS includes the mass of both algal and nonalgal particles, and is not a clear indicator of the nonalgal particle concentration $C_{nap}$.

Our field data were complemented by other fluorescence amplitude values retrieved from results of field campaigns by Roesler and Perry [19]. We considered two of their data sets which are identified as “Coastal Environment” and “Estuarine Environment”. The first set was acquired in the Gulf of Maine and along the Oregon coast with [Chl] = 0.5 – 2.8 $mg/m^3$. Their reflectance spectra, when analyzed, clearly corresponded to low CDOM concentrations. Both locations were close to the open ocean. The second dataset was acquired in Puget Sound, Washington with reflectances corresponding to higher CDOM effects and with

#87554 - $15.00 USD Received 14 Sep 2007; revised 6 Nov 2007; accepted 6 Nov 2007; published 12 Nov 2007

features more typical of case 2 waters. In that paper, fluorescence amplitudes were presented in irradiance reflectance units. Therefore, to compare them with our fluorescence data in radiance units above the water, we multiplied their values by $0.53\,E_d / Q$ , using $Q$ = 4.0 as a reasonable estimate [43].

The relationships between fluorescence magnitude and [Chl] from all sets of field measurements are shown in Fig. 9 and compared with Eqs. (19) for datasets 1 and 2. These expressions, we recall, are designed to illustrate the "average" and extreme water conditions regarding NAP scattering and CDOM observed in our simulation studies.

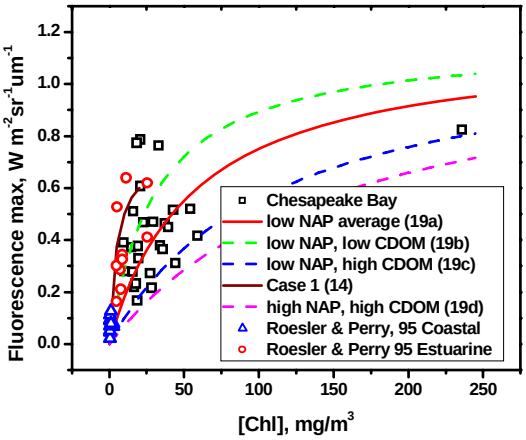


Fig. 9. Comparison of field fluorescence amplitude data from Chesapeake Bay and other areas [19], expression (14) for case 1 waters, expressions (19) from HYDROLIGHT simulated datasets as a function of [Chl].

It can be seen that within our Chesapeake Bay data, most of the points are inside or very close to the boundaries determined from our simulations, confirming that the data can be represented using a much smaller range in quantum yield. Sporadic higher or lower values might be attributable to either higher variability in the absorption spectra compared to values in data sets 1 and 2, or variations in fluorescence quantum yield. As expected, the "Coastal Environment" data [19] were very close to the fluorescence – [Chl] dependence for case 1 waters, while the "Estuarine Environment" data [19] fall mostly between the case 1 water curve and our estimated case 2 waters with low NAPs and low CDOM. It is obvious that some deviations from the models exist.

In classifying the Chesapeake water conditions, statistics on $a_y(400)$ and TSS concentrations for the Chesapeake Bay stations for which fluorescence was retrieved is shown in Fig. 10. TSS values are not directly related to the concentrations of nonalgal particles, but since contribution of nonalgal particles to attenuation is relatively small (18b), this statistics once again makes reasonable grouping of $Fl$ values around curve of expression (19a) in Fig. 9 which corresponds to the moderate values of $a_y(400)$ and TSS.

#87554 - $15.00 USD Received 14 Sep 2007; revised 6 Nov 2007; accepted 6 Nov 2007; published 12 Nov 2007

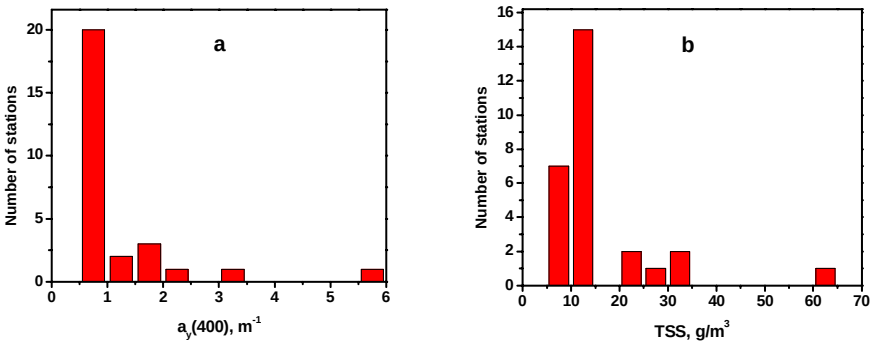


Fig. 10. Statistics for the Chesapeake Bay stations data from which were used in Fig. 9(a) $a_y(400)$, b) TSS concentrations.

Taking into account the wide range of conditions at our Chesapeake bay stations, with [Chl] = 9.1 – 235 mg/m$^3$, $a_y(400)$ = 0.55 – 5.6 m$^{-1}$, TSS concentrations 7 – 64.8 g/m$^3$, salinity 1.8 – 12 ‰, clear sky to hazy and cloudy conditions, data added from three other locations and water conditions [19] and rough assumptions for the $Q$ parameter and fluorescence quantum yield, we believe the resultant consistency between our datasets and the $\eta = 1\%$ regime should be considered excellent. We stress again that all fluorescence amplitude values are presented in radiance units and were calculated from the reflectance measurements and simulations by multiplication using $E_d$ =1.1 Wm$^{-2}$ nm$^{-1}$. For conditions other than clear sky, this factor should be chosen appropriately.

Our results clearly show that in coastal waters, the high variability observed in fluorescence amplitude for fixed [Chl] values, which are often attributed to high quantum yield variability, should be attributed instead mostly to effects of strong absorption by phytoplankton and CDOM and scattering by NAPs. Together, these can change fluorescence amplitude for [Chl] = 1 - 50 mg/m$^3$ by a factor of 3 – 10. Smaller values of specific chlorophyll absorption [38] also contribute significantly to the lower fluorescence magnitudes in the coastal environment in comparison with the open ocean assuming proportionality between PAR and $a^*_{Chl}$.

We would like to stress that the results of comparison of the model and field measurements is limited to show that data derived from field measurements fall inside the boundaries predicted by our radiative transfer model simulations and that expression (19a) can on average be a good estimation of the fluorescence amplitude. In fact, there are many factors which make point-point comparison of the model and field data unreasonable. These include true (versus apparent) variability in the fluorescence quantum yield, spatial and temporal shifts between reflectance and WET Labs measurements which resulted in some changes of water conditions, the 4 nm resolution of WET Labs data in comparison with 1 nm reflectance data which can miss fine features on the spectra, unknown actual specific chlorophyll absorption spectra and complex illumination conditions. Much more detailed and accurate field studies are needed to evaluate the applicability of expression (18) which explicitly relates $Fl$ to [Chl], CDOM absorption and $C_{nap}$ in a point-point fashion. On the other hand we found that if graphs in Fig. 9 were simulated with fluorescence quantum yield $\eta$ = 0.5% and 2% instead of 1% with respective decrease and increase of $Fl$ in (19), the experimental data would be completely outside modeled boundaries. This makes clear that

#87554 - $15.00 USD Received 14 Sep 2007; revised 6 Nov 2007; accepted 6 Nov 2007; published 12 Nov 2007

despite many uncertainties mentioned above the $\eta$ = 1% hypothesis in a statistical sense should be considered highly probable and the resultant $Fl$ model is a good first approximation of fluorescence in coastal waters.

*4.5 Contribution of fluorescence to the NIR reflectance peak*

To determine the contribution of the fluorescence to the total NIR peak, we calculate the ratio of the fluorescence peak to the total reflectance at 695 nm, which is usually close to the maximum reflectance in the NIR for our datasets 1 and 2 (low NAP and high NAP cases). As shown in Fig. 11(a) for the low NAP case, the fluorescence magnitude is 10-30% of the peak magnitude for our range of [Chl], so its contribution is significant and its value should be distinguishable from total reflectance. However, in the high NAP case Fig. 11(b) the contribution of the fluorescence decreased rapidly with increasing NAP concentrations, due to the relative increase of elastic scattering reflectance. For $C_{nap}$ > 10 g/m$^3$, the contribution of fluorescence to the total peak dropped below 5% and could be ignored in most applications and retrieval algorithms. Even for $C_{nap}$ = 2 – 10 g/m$^3$ the fluorescence contribution is still below 10% of the peak, making its retrieval questionable.

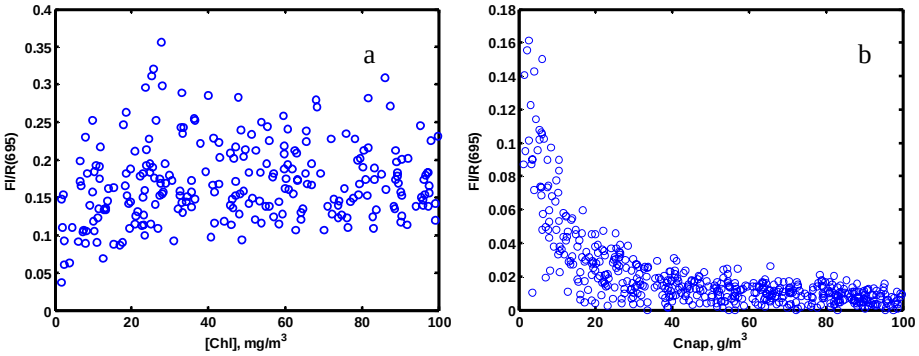


Fig. 11. Ratio of Fl/$R_{rs}$(695) (a) as a function of [Chl] and (b) as a function of NAP concentration

Relationships between fluorescence amplitudes and concentrations of water constituents developed by us (18)-(19) can be used directly to estimate $Fl$ values (or corresponding components in reflectances) if [Chl], $a_y(400)$ and $C_{nap}$ are known. They can also be applied to algorithms for the retrieval of IOP and water parameters from reflectance spectra. As a first step, these retrievals can be carried out without taking into account the fluorescence component to make preliminary estimation of [Chl], $a_y(400)$ and $C_{nap}$ values. These retrievals then can be repeated after calculation and allowance for fluorescence amplitude. This approach also allows one to separate open ocean and coastal waters and to choose an appropriate expression (14) or (18b) for fluorescence amplitude estimation. On the other hand, if the type of water is known in advance, expressions (14) or (18b) can be incorporated into a retrieval algorithm as an additional constraint.

## 5. Conclusions

Datasets with more than 2000 reflectances typical for coastal waters, with high variability of [Chl], CDOM, and NAPs, together with specific chlorophyll absorption spectra and spectral distributions of attenuation and scattering and with results of comprehensive measurements in Chesapeake Bay were used to analyze the magnitude of fluorescence in coastal waters and its dependence on [Chl] and other water components.

#87554 - $15.00 USD Received 14 Sep 2007; revised 6 Nov 2007; accepted 6 Nov 2007; published 12 Nov 2007

Based on these HYDROLIGHT simulations we first found that the fluorescence amplitude in coastal waters is in general substantially lower for the same [Chl] than in the open ocean. This is due to the decrease of photosynthetically available radiation (PAR), attenuated by absorption of CDOM and/or absorption and backscattering of NAPs. This decrease was especially noticeable for [Chl] < 50 mg/m$^3$, where fluorescence can be 3-10 times lower than in the open ocean. To facilitate our comparisons, we developed parameterized expressions to quantify the fluorescence amplitude as a function of [Chl] as well as CDOM and NAP concentrations

Using our models within appropriate limits and comparing experimental relations between $Fl$ and [Chl] to our model estimates, we found that the variability of fluorescence magnitude in coastal waters can best be attributed to attenuation effects by water constituents, rather than to the differences in fluorescence quantum yield which we found to be well approximated at around $\eta$ = 1.0% and consistent to field measurement estimates in case 1 waters. In fact, we found that this value of the quantum yield best explains the change in the NIR reflectance maximum wavelength as a function of [Chl]. Our simulations showed that higher $\eta$ values corresponding to higher fluorescence magnitudes would result in unrealistically small total reflectance shifts of the peak in the NIR from 685 nm with increasing [Chl] which are not observed in the field and unrealistically small shifts if the quantum efficiency is too low.

In addition to the intrinsic value in interpreting our field measurements, the simple parameterized fluorescence expressions can be integrated into existing algorithms for [Chl] and IOP retrieval from reflectance spectra and will presumably improve algorithms which are based on reflectance peak characteristics in the NIR spectral zone.

Finally, our calculations also show that NAP concentration is a critical factor in the contribution of fluorescence to the total reflectance in the NIR. For low NAP concentrations $C_{nap}$ < 2 g/m$^3$, the fluorescence reflectance component contributes 10-30% to the total reflectance in the NIR, which can affect retrieval algorithms unless they are separated using proper techniques and methods from the elastic reflectance. However, with increasing NAP concentration, the fluorescence contribution decreases rapidly because elastic reflectance increases almost proportionally to $C_{nap}$ as well as the additional attenuation by NAPs. In those cases, including many estuarine and near shore conditions, as well as turbid inland waters, the effect of fluorescence on reflectance spectra is almost negligible.

**Acknowledgments**

We would like to thank the following individuals who assisted in field and laboratory measurements: A. Binderup, R. Carlson, L. Chasar, E. Cizek, K. Dillon, B. Elmaanaoui, C. Fan, C. Hladik, C. Holland, R. LaCouture, M. Machmuller, J. Mulder, A. Mustapha, S. Pasko, M. Vargas, and L.Whitehurst. Laboratory facilities and other logistical support for the Chesapeake Bay campaign, including two research boats, were generously provided by K. Clark from Morgan State University's Estuarine Research Center at Solomon, MD and by J. Bortz at the Maryland Department of Natural Resources. We are also very grateful to the reviewers of the paper whose comments and suggestions helped to improve it significantly.

This research was supported partially by grants from NASA #NCC-1-03009 and NOAA #NA06OAR4810162 and #NA17AE1624 with subcontracts from Environmental Cooperative Science Center, Florida A&M University.

#87554 - $15.00 USD Received 14 Sep 2007; revised 6 Nov 2007; accepted 6 Nov 2007; published 12 Nov 2007